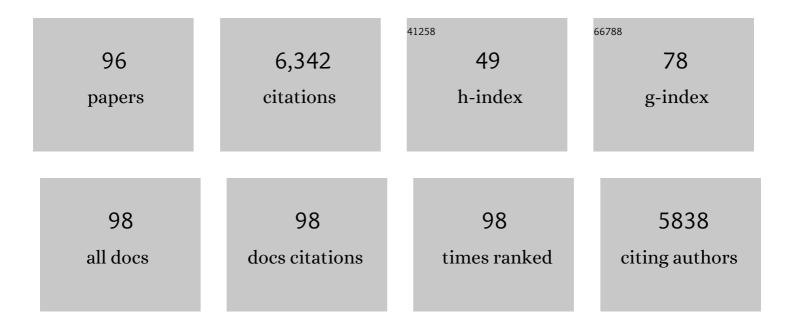
List of Publications by Year in descending order

Source: https://exaly.com/author-pdf/1521648/publications.pdf Version: 2024-02-01



#	Article	IF	CITATIONS
1	Ultrasonically assisted hydrothermal synthesis of activated carbon–HKUST-1-MOF hybrid for efficient simultaneous ultrasound-assisted removal of ternary organic dyes and antibacterial investigation: Taguchi optimization. Ultrasonics Sonochemistry, 2016, 31, 383-393.	3.8	267
2	Modeling of quaternary dyes adsorption onto ZnO–NR–AC artificial neural network: Analysis by derivative spectrophotometry. Journal of Industrial and Engineering Chemistry, 2016, 34, 186-197.	2.9	240
3	Sonochemical-assisted synthesis of CuO/Cu2O/Cu nanoparticles as efficient photocatalyst for simultaneous degradation of pollutant dyes in rotating packed bed reactor: LED illumination and central composite design optimization. Ultrasonics Sonochemistry, 2018, 40, 601-610.	3.8	202
4	Facile Synthesis of Mixed Metal–Organic Frameworks: Electrode Materials for Supercapacitors with Excellent Areal Capacitance and Operational Stability. ACS Applied Materials & Interfaces, 2018, 10, 23063-23073.	4.0	199
5	Simultaneous ultrasound-assisted ternary adsorption of dyes onto copper-doped zinc sulfide nanoparticles loaded on activated carbon: Optimization by response surface methodology. Spectrochimica Acta - Part A: Molecular and Biomolecular Spectroscopy, 2015, 145, 203-212.	2.0	182
6	Synthesis of magnetic γ-Fe2O3-based nanomaterial for ultrasonic assisted dyes adsorption: Modeling and optimization. Ultrasonics Sonochemistry, 2016, 32, 418-431.	3.8	174
7	Screening and optimization of highly effective ultrasound-assisted simultaneous adsorption of cationic dyes onto Mn-doped Fe3O4-nanoparticle-loaded activated carbon. Ultrasonics Sonochemistry, 2017, 34, 1-12.	3.8	165
8	Highly efficient simultaneous ultrasonic assisted adsorption of brilliant green and eosin B onto ZnS nanoparticles loaded activated carbon: Artificial neural network modeling and central composite design optimization. Spectrochimica Acta - Part A: Molecular and Biomolecular Spectroscopy, 2016, 153, 257-267.	2.0	160
9	Application of central composite design for simultaneous removal of methylene blue and Pb2+ ions by walnut wood activated carbon. Spectrochimica Acta - Part A: Molecular and Biomolecular Spectroscopy, 2015, 135, 479-490.	2.0	149
10	Photocatalytic degradation of binary mixture of toxic dyes by HKUST-1 MOF and HKUST-1-SBA-15 in a rotating packed bed reactor under blue LED illumination: central composite design optimization. RSC Advances, 2016, 6, 17204-17214.	1.7	140
11	Ultrasound-assisted binary adsorption of dyes onto Mn@ CuS/ZnS-NC-AC as a novel adsorbent: Application of chemometrics for optimization and modeling. Journal of Industrial and Engineering Chemistry, 2017, 54, 377-388.	2.9	137
12	Rapid removal of Auramine-O and Methylene blue by ZnS:Cu nanoparticles loaded on activated carbon: A response surface methodology approach. Journal of the Taiwan Institute of Chemical Engineers, 2015, 53, 80-91.	2.7	136
13	Enhanced simultaneous removal of malachite green and safranin O by ZnO nanorod-loaded activated carbon: modeling, optimization and adsorption isotherms. New Journal of Chemistry, 2015, 39, 7998-8005.	1.4	130
14	Ternary dye adsorption onto MnO ₂ nanoparticle-loaded activated carbon: derivative spectrophotometry and modeling. RSC Advances, 2015, 5, 72300-72320.	1.7	129
15	Achieving enhanced blue-light-driven photocatalysis using nanosword-like VO2/CuWO4 type II n–n heterojunction. Chemical Engineering Journal, 2018, 339, 189-203.	6.6	123
16	Preparation of nanomaterials for the ultrasound-enhanced removal of Pb2+ ions and malachite green dye: Chemometric optimization and modeling. Ultrasonics Sonochemistry, 2017, 34, 677-691.	3.8	121
17	Performance of CuS nanoparticle loaded on activated carbon in the adsorption of methylene blue and bromophenol blue dyes in binary aqueous solutions: Using ultrasound power and optimization by central composite design. Journal of Molecular Liquids, 2016, 219, 667-676.	2.3	118
18	Central composite design and genetic algorithm applied for the optimization of ultrasonic-assisted removal of malachite green by ZnO Nanorod-loaded activated carbon. Spectrochimica Acta - Part A: Molecular and Biomolecular Spectroscopy, 2016, 167, 157-164.	2.0	114

#	Article	IF	CITATIONS
19	Sonochemical assisted hydrothermal synthesis of ZnO: Cr nanoparticles loaded activated carbon for simultaneous ultrasound-assisted adsorption of ternary toxic organic dye: Derivative spectrophotometric, optimization, kinetic and isotherm study. Ultrasonics Sonochemistry, 2016, 32, 119-131.	3.8	110
20	Ultrasound-assisted removal of Al ³⁺ ions and Alizarin red S by activated carbon engrafted with Ag nanoparticles: central composite design and genetic algorithm optimization. RSC Advances, 2015, 5, 59522-59532.	1.7	109
21	BiPO ₄ /Bi ₂ S ₃ -HKUST-1-MOF as a novel blue light-driven photocatalyst for simultaneous degradation of toluidine blue and auramine-O dyes in a new rotating packed bed reactor: optimization and comparison to a conventional reactor. RSC Advances, 2016, 6, 63667-63680.	1.7	103
22	Saccharomyces cerevisiae for the biosorption of basic dyes from binary component systems and the high order derivative spectrophotometric method for simultaneous analysis of Brilliant green and Methylene blue. Journal of Industrial and Engineering Chemistry, 2013, 19, 227-233.	2.9	96
23	Preparation and characterization of MWCNTs functionalized by N-(3-nitrobenzylidene)-Nâ€2-trimethoxysilylpropyl-ethane-1,2-diamine for the removal of aluminum(<scp>iii</scp>) ions via complexation with eriochrome cyanine R: spectrophotometric detection and optimization. RSC Advances. 2015. 5. 61060-61069.	1.7	94
24	Ag 3 PO 4 /AgBr/Ag-HKUST-1-MOF composites as novel blue LED light active photocatalyst for enhanced degradation of ternary mixture of dyes in a rotating packed bed reactor. Chemical Engineering and Processing: Process Intensification, 2017, 114, 24-38.	1.8	94
25	Synthesis of nickel sulfide nanoparticles loaded on activated carbon as a novel adsorbent for the competitive removal of Methylene blue and Safranin-O. Spectrochimica Acta - Part A: Molecular and Biomolecular Spectroscopy, 2014, 123, 402-409.	2.0	93
26	A simple ultrasensitive electrochemical sensor for simultaneous determination of gallic acid and uric acid in human urine and fruit juices based on zirconia-choline chloride-gold nanoparticles-modified carbon paste electrode. Biosensors and Bioelectronics, 2018, 114, 30-36.	5.3	93
27	Local, cheep and nontoxic activated carbon as efficient adsorbent for the simultaneous removal of cadmium ions and malachite green: Optimization by surface response methodology. Journal of Industrial and Engineering Chemistry, 2015, 21, 760-767.	2.9	91
28	Modeling and optimization of simultaneous removal of ternary dyes onto copper sulfide nanoparticles loaded on activated carbon using second-derivative spectrophotometry. Journal of the Taiwan Institute of Chemical Engineers, 2016, 65, 212-224.	2.7	91
29	CoxZn1â^'x ZIF-derived binary Co3O4/ZnO wrapped by 3D reduced graphene oxide for asymmetric supercapacitor: Comparison of pure and heat-treated bimetallic MOF. Ceramics International, 2017, 43, 14413-14425.	2.3	91
30	New ion-imprinted polymer-functionalized mesoporous SBA-15 for selective separation and preconcentration of Cr(<scp>iii</scp>) ions: modeling and optimization. RSC Advances, 2015, 5, 105789-105799.	1.7	90
31	Synthesis of ZnO-nanorod-based materials for antibacterial, antifungal activities, DNA cleavage and efficient ultrasound-assisted dyes adsorption. Ecotoxicology and Environmental Safety, 2017, 142, 330-337.	2.9	84
32	Simultaneous removal of methylene blue and Pb ²⁺ ions using ruthenium nanoparticle-loaded activated carbon: response surface methodology. RSC Advances, 2015, 5, 83427-83435.	1.7	83
33	Rapid adsorption of ternary dye pollutants onto copper (I) oxide nanoparticle loaded on activated carbon: Experimental optimization via response surface methodology. Journal of Environmental Chemical Engineering, 2016, 4, 1769-1779.	3.3	82
34	Application of chitosan-citric acid nanoparticles for removal of chromium (VI). International Journal of Biological Macromolecules, 2015, 80, 431-444.	3.6	79
35	Photo-Sensitive Pb5S2I6 crystal incorporated polydopamine biointerface coated on nanoporous TiO2 as an efficient signal-on photoelectrochemical bioassay for ultrasensitive detection of Cr(VI) ions. Biosensors and Bioelectronics, 2019, 132, 105-114.	5.3	76
36	L-phenylalanine-imprinted polydopamine-coated CdS/CdSe n-n type II heterojunction as an ultrasensitive photoelectrochemical biosensor for the PKU monitoring. Biosensors and Bioelectronics, 2020, 165, 112346.	5.3	76

#	Article	IF	CITATIONS
37	Novel nanorose-like Ce(<scp>iii</scp>)-doped and undoped Cu(<scp>ii</scp>)–biphenyl-4,4-dicarboxylic acid (Cu(<scp>ii</scp>)–BPDCA) MOSs as visible light photocatalysts: synthesis, characterization, photodegradation of toxic dyes and optimization. Physical Chemistry Chemical Physics, 2016, 18, 11278-11287.	1.3	73
38	Random forest model for the ultrasonic-assisted removal of chrysoidine G by copper sulfide nanoparticles loaded on activated carbon; response surface methodology approach. RSC Advances, 2015, 5, 59335-59343.	1.7	72
39	Preparation and characterization of an ACaE Fe ₃ 0 ₄ aE Au hybrid for the simultaneous removal of Cd ²⁺ , Pb ²⁺ , Cr ³⁺ and Ni ²⁺ ions from aqueous solution via complexation with 2-((2,4-dichloro-benzylidene)-amino)-benzenethiol: Taguchi optimization. RSC Advances, 2016, 6,	1.7	67
40	Equilibrium, kinetic and isotherm of some metal ion biosorption. Journal of Industrial and Engineering Chemistry, 2013, 19, 987-992.	2.9	66
41	Controlled thermolysis of MIL-101(Fe, Cr) for synthesis of FexOy/porous carbon as negative electrode and Cr2O3/porous carbon as positive electrode of supercapacitor. Applied Surface Science, 2019, 469, 192-203.	3.1	62
42	Competitive adsorption of Direct Yellow 12 and Reactive Orange 12 on ZnS:Mn nanoparticles loaded on activated carbon as novel adsorbent. Journal of Industrial and Engineering Chemistry, 2014, 20, 564-571.	2.9	58
43	Experimental design for simultaneous analysis of malachite green and methylene blue; derivative spectrophotometry and principal component-artificial neural network. RSC Advances, 2015, 5, 38939-38947.	1.7	58
44	Cobalt terephthalate MOF-templated synthesis of porous nano-crystalline Co3O4 by the new indirect solid state thermolysis as cathode material of asymmetric supercapacitor. Physica E: Low-Dimensional Systems and Nanostructures, 2017, 94, 158-166.	1.3	58
45	Ti-Based Solid-State Imprinted-Cu2O/CuInSe2 Heterojunction Photoelectrochemical platform for Highly Selective Dopamine Monitoring. Sensors and Actuators B: Chemical, 2021, 326, 128824.	4.0	58
46	Ionic liquid-based ordered mesoporous organosilica-supported copper as a novel and efficient nanocatalyst for the one-pot synthesis of Biginelli products. Microporous and Mesoporous Materials, 2015, 204, 269-275.	2.2	54
47	Synthesis of regenerable Zn(OH) ₂ nanoparticle-loaded activated carbon for the ultrasound-assisted removal of malachite green: optimization, isotherm and kinetics. RSC Advances, 2015, 5, 79119-79128.	1.7	53
48	Characterization of Au nano-cluster formation on and diffusion in polystyrene using XPS peak shape analysis. Surface Science, 2007, 601, 3261-3267.	0.8	50
49	Noise reduction procedures applied to XPS imaging of depth distribution of atoms on the nanoscale. Surface Science, 2008, 602, 3064-3070.	0.8	50
50	Highly selective few-ppm NO gas-sensing based on necklace-like nanofibers of ZnO/CdO n-n type I heterojunction. Sensors and Actuators B: Chemical, 2019, 297, 126774.	4.0	50
51	Fabrication of hybrid supercapacitor based on rod-like HKUST-1@polyaniline as cathode and reduced graphene oxide as anode. Physica E: Low-Dimensional Systems and Nanostructures, 2018, 99, 16-23.	1.3	49
52	Sensitive, selective and rapid ammonia-sensing by gold nanoparticle-sensitized V2O5/CuWO4 heterojunctions for exhaled breath analysis. Applied Surface Science, 2020, 501, 144270.	3.1	49
53	Nano-sized molecularly imprinted polymer for selective ultrasound-assisted microextraction of pesticide Carbaryl from water samples: Spectrophotometric determination. Journal of Colloid and Interface Science, 2017, 498, 313-322.	5.0	47
54	Validity of Yubero-Tougaard theory to quantitatively determine the dielectric properties of surface nanofilms. Physical Review B, 2008, 77, .	1.1	46

#	Article	IF	CITATIONS
55	Preparation of Iodide Selective Carbon Paste Electrode with Modified Carbon Nanotubes by Potentiometric Method and Effect of CuSâ€NPs on Its Response. Electroanalysis, 2015, 27, 1516-1522.	1.5	46
56	Application of high order derivative spectrophotometry to resolve the spectra overlap between BG and MB for the simultaneous determination of them: Ruthenium nanoparticle loaded activated carbon as adsorbent. Journal of Industrial and Engineering Chemistry, 2014, 20, 2421-2427.	2.9	45
57	XPS for non-destructive depth profiling and 3D imaging of surface nanostructures. Analytical and Bioanalytical Chemistry, 2010, 396, 2741-2755.	1.9	42
58	A novel polyvinyl chloride-membrane optical sensor for the determination of Cu2+ ion based on synthesized ($N\hat{a}\in^21E,N\hat{a}\in^22E$)- $N\hat{a}\in^21,N\hat{a}\in^22$ -bis(pyridine-2-ylmethylene)oxalohydrazide: Experimental design and optimization. Spectrochimica Acta - Part A: Molecular and Biomolecular Spectroscopy, 2015, 138, 878-884.	2.0	37
59	Removal of methyl orange by multiwall carbon nanotube accelerated by ultrasound devise: Optimized experimental design. Advanced Powder Technology, 2015, 26, 1087-1093.	2.0	36
60	Highly selective MXene/V2O5/CuWO4-based ultra-sensitive room temperature ammonia sensor. Journal of Hazardous Materials, 2021, 416, 126196.	6.5	36
61	Molecular Imprinted Poly(2,5-benzimidazole)-Modified VO ₂ –CuWO ₄ Homotype Heterojunction for Photoelectrochemical Dopamine Sensing. Analytical Chemistry, 2022, 94, 6781-6790.	3.2	35
62	Design and construction of ZIF(8 and 67) supported Fe3O4 composite as advanced materials of high performance supercapacitor. Physica E: Low-Dimensional Systems and Nanostructures, 2021, 126, 114442.	1.3	32
63	XPS imaging of depth profiles and amount of substance based on Tougaard's algorithm. Surface Science, 2006, 600, 3015-3021.	0.8	29
64	A novel PVC-membrane optical sensor for high sensitive and selective determination of Cu2+ ion based on synthesized (E)-N′-(pyridin-2-ylmethylene)isonicotin-ohydrazide. Journal of Molecular Liquids, 2014, 199, 483-488.	2.3	29
65	Efficient adsorption of Europhtal onto activated carbon modified with ligands (1E,2E)-1,2-bis(pyridin-4-ylmethylene)hydrazine (M) and (1E,2E)-1,2-bis(pyridin-3-ylmethylene)hydrazine (SCH-4); response surface methodology. RSC Advances, 2015, 5, 42376-42387.	1.7	26
66	Removal of methylene blue from aqueous solution by walnut carbon: optimization using response surface methodology. Desalination and Water Treatment, 2016, 57, 3179-3193.	1.0	25
67	Nondestructive quantitative XPS imaging of depth distribution of atoms on the nanoscale. Surface and Interface Analysis, 2008, 40, 688-691.	0.8	23
68	Simultaneous extraction and preconcentration of Cu2+, Ni2+ and Zn2+ ions using Ag nanoparticle-loaded activated carbon: Response surface methodology. Advanced Powder Technology, 2016, 27, 426-435.	2.0	23
69	In-situ growth of ultrathin Ni6MnO8 nanosheets on nickel foam as a binder-free positive electrode for asymmetric supercapacitor: Effects of alkaline aqueous and redox additive electrolytes. Journal of Molecular Liquids, 2017, 244, 269-278.	2.3	23
70	One-pot electrochemical growth of sponge-like polyaniline-intercalated phosphorous-doped graphene oxide on nickel foam as binder-free electrode material of supercapacitor. Physica E: Low-Dimensional Systems and Nanostructures, 2018, 100, 45-53.	1.3	23
71	SnO2 nanoparticle-loaded activated carbon for simultaneous removal of Acid Yellow 41 and Sunset Yellow; derivative spectrophotometric, artificial neural network and optimization approach. Spectrochimica Acta - Part A: Molecular and Biomolecular Spectroscopy, 2015, 150, 1002-1012.	2.0	21
72	A new silver (I) ions optical sensor based on nanoporous thin films of sol–gel by rose bengal dye. Sensors and Actuators B: Chemical, 2018, 259, 20-29.	4.0	21

#	Article	IF	CITATIONS
73	High-rate supercapacitor based on NiCo-MOF-derived porous NiCoP for efficient energy storage. Journal of Materials Science: Materials in Electronics, 2021, 32, 13117-13128.	1.1	19
74	Synthesis and characterization of antibacterial chromium iron oxide nanoparticleâ€loaded activated carbon for ultrasoundâ€assisted wastewater treatment. Applied Organometallic Chemistry, 2018, 32, e3981.	1.7	18
75	S-scheme NIR-edge Ag3CuS2/VO2 heterostructure for photo-oxidation/reduction of methylene blue/Cr (VI). Applied Surface Science, 2022, 590, 153118.	3.1	18
76	Reducing thermal contact resistance using nanocoating. Applied Thermal Engineering, 2014, 70, 641-646.	3.0	16
77	Non-Destructive Depth Profiling by XPS Peak Shape Analysis. Journal of Surface Analysis (Online), 2009, 15, 220-224.	0.1	15
78	Synthesis and electrochemical properties of Mg-doped chromium-based metal organic framework/reduced graphene oxide composite for supercapacitor application. Journal of Materials Science: Materials in Electronics, 2018, 29, 8421-8430.	1.1	14
79	Colorimetric determination of F-, Br- and I- ions by Ehrlich's bio-reagent oxidation over enzyme mimic like gold nanoparticles: Peroxidase-like activity and multivariate optimization. Spectrochimica Acta - Part A: Molecular and Biomolecular Spectroscopy, 2020, 226, 117606.	2.0	14
80	Reflection electron energy loss spectroscopy as efficient technique for the determination of optical properties of polystyrene intermixed with gold nanoparticles. Applied Surface Science, 2017, 392, 697-700.	3.1	13
81	Hierarchical Fe ₂ O ₃ /Na ₂ WO ₄ Nanofibers Supported on Conductive Carbon Cloth as a High-Performance Supercapacitor. Energy & Fuels, 2021, 35, 11551-11562.	2.5	13
82	Schiff Base Impregnated Plasticized Polyvinyl Chloride Optical Sensor for Selective and Efficient Detection of Copper (II) Ion: Central Composite Design. IEEE Sensors Journal, 2015, 15, 6604-6610.	2.4	11
83	Simultaneous removal of Cu ²⁺ and Cr ³⁺ ions from aqueous solution based on Complexation with Eriochrome cyanineâ€R and derivative spectrophotometric method. Applied Organometallic Chemistry, 2018, 32, e3918.	1.7	11
84	Impact of silver incorporation on cobalt rich 3-D porous carbon arising from solid state thermolysis of ZIF-67 as a pseudocapacitor electrode: Improvement of diffusion-controlled charge storage. Solid State Ionics, 2021, 368, 115697.	1.3	10
85	Determination of electronic properties of nanostructures using reflection electron energy loss spectroscopy: Nano-metalized polymer as case study. Applied Surface Science, 2016, 377, 44-47.	3.1	9
86	Surfactantâ€directed oneâ€pot preparation of novel Tiâ€containing mesomaterial with improved catalytic activity and reusability. Applied Organometallic Chemistry, 2018, 32, e4471.	1.7	9
87	Comparative studies on electrochemical energy storage of NiFe-S nanoflake and NiFe-OH towards aqueous supercapacitor. Journal of Materials Science: Materials in Electronics, 2019, 30, 4499-4510.	1.1	8
88	Improvement in the performance of a zinc ion-selective potentiometric sensor using modified core/shell Fe3O4@SiO2nanoparticles. RSC Advances, 2015, 5, 105925-105933.	1.7	7
89	Electrophoretic deposition of mixed copper oxide/GO as cathode and N-doped GO as anode for electrochemical energy storage. Electrochimica Acta, 2018, 268, 392-402.	2.6	7
90	Ru-containing magnetic yolk–shell structured nanocomposite: a powerful, recoverable and highly durable nanocatalyst. RSC Advances, 2021, 11, 10243-10252.	1.7	6

#	Article	IF	CITATIONS
91	Three-Dimensional X-Ray Photoelectron Tomography on the Nanoscale: Limits of Data Processing by Principal Component Analysis. Microscopy and Microanalysis, 2013, 19, 751-760.	0.2	5
92	Photocatalytic degradation of disulfine blue using titanium dioxide nanoparticles under ultraviolet light irradiation: A response surface methodology approach. Environmental Progress and Sustainable Energy, 2016, 35, 1657-1663.	1.3	5
93	Morphology control of Ni doped rod like MIL-88A derived FeS2 embedded in nitrogen-rich carbon as an efficient electrocatalyst for the oxygen reduction reaction. Journal of Molecular Structure, 2021, 1237, 130329.	1.8	5
94	Synthesis of rod-like ternary Cu(Cd)-In-S and quaternary Cu-Cd-In-S by controlled ion exchange of MIL-68(In) derived indium sulfide for high energy-storage capacitor. Synthetic Metals, 2021, 278, 116815.	2.1	5
95	Co-electrophoretic deposition of Mn2O3/activated carbon on CuO nanowire array growth on copper foam as a binder-free electrode for high-performance supercapacitors. Journal of Materials Science: Materials in Electronics, 2021, 32, 27268-27278.	1.1	4
96	Investigation on the dielectric properties of titanium-loaded ionic liquid-based nano-organosilica as a novel material. Advanced Powder Technology, 2018, 29, 813-817.	2.0	1